THE ART OF SCIENTIFIC STORYTELLING: CRAFTING COMPELLING STEM PRESENTATIONS

Dr. Mark Jensen
Department of Chemistry
Concordia College
Moorhead, MN

CONCORDIA COLLEGE
MOORHEAD, MINNESOTA


HARPER LEE
TO KILL A Mockingbird
A NOVEL BY
HARPER LEE
LIPPINCOTT
WALT DISNEY PICTURES PRESENTS
THE LION KING
THE LORD OF THE RINGS
THE FELLOWSHIP OF THE RING
THE ODYSSEY
HOMER
PRIDE AND PREJUDICE
ILLUSTRATED EDITION
TWENTIETH CENTURY-FOX Presents A LUCASFILM LTD. PRODUCTION
STAR WARS
Starring MARK HAMILL HARRISON FORD CARRIE FISHER
PETER CUSHING
and
ALEC GUINNESS
Written and Directed by
GEORGE LUCAS
Produced by
GARY KURTZ
Music by
JOHN WILLIAMS
PANAVISION®
PRINTS BY DE LUXE®
TECHNICOLOR®
DOLBY SYSTEM
ROMEO and JULIET
WILLIAM SHAKESPEARE
MAPLE CLASSICS
J.
Harry Potter
and the Sorcerer's Stone
SCHOLASTIC
A Tale of Two Cities
Charles Dickens
BELOVED
TONI MORRISON

RESEARCH

CELL BIOLOGY

ESCRT-mediated membrane repair protects tumor-derived cells against T cell attack

Alex T. Ritter[1]*, Gleb Shtengel[2], C. Shan Xu[2], Aubrey Weigel[2], David P. Hoffman[2]†, Melanie Freeman[2]†, Nirmala Iyer[2], Nensi Alivodej[2]‡, David Ackerman[2], Ilia Voskoboinik[3], Joseph Trapani[3], Harald F. Hess[2], Ira Mellman[1]*

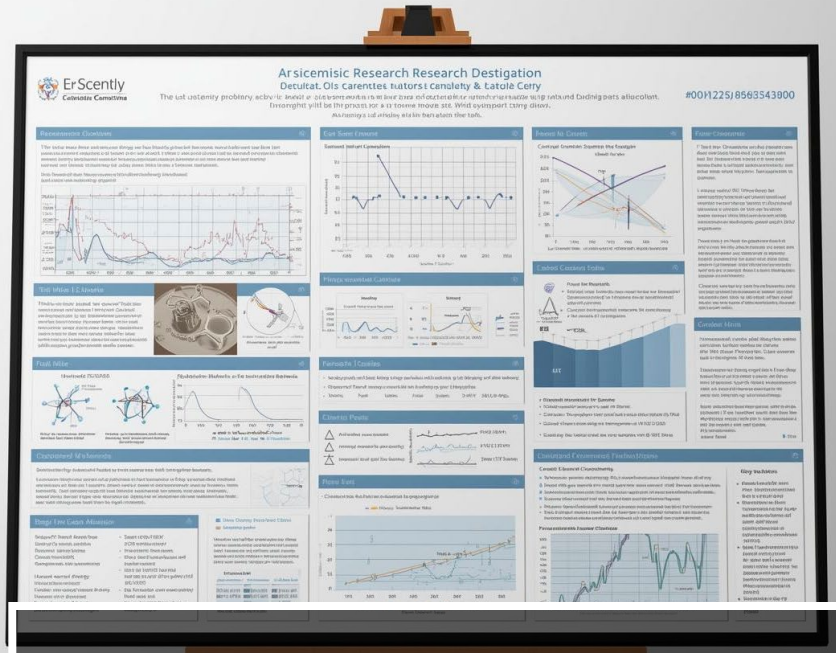

WHERE DO SCIENTISTS TELL STORIES?

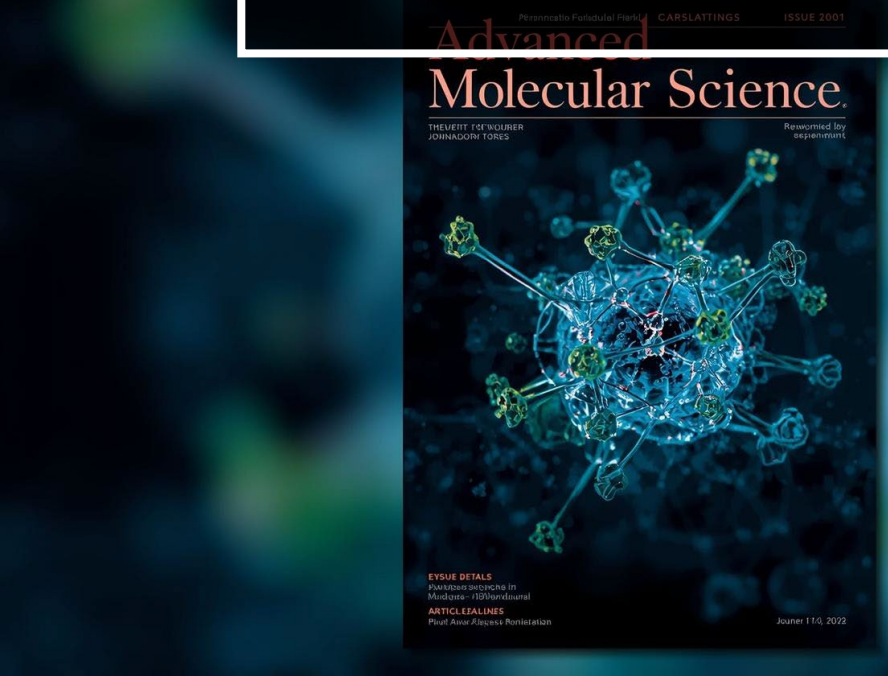

Your Brain on Stories

Neural Coupling
Stories synchronize the listener's brain with the storyteller's brain

Mirroring
Mirror neurons allow listeners to mirror experience

Cortical Activity
Stories activate several areas of the brain such as the motor cortex, sensory cortex, and frontal cortex

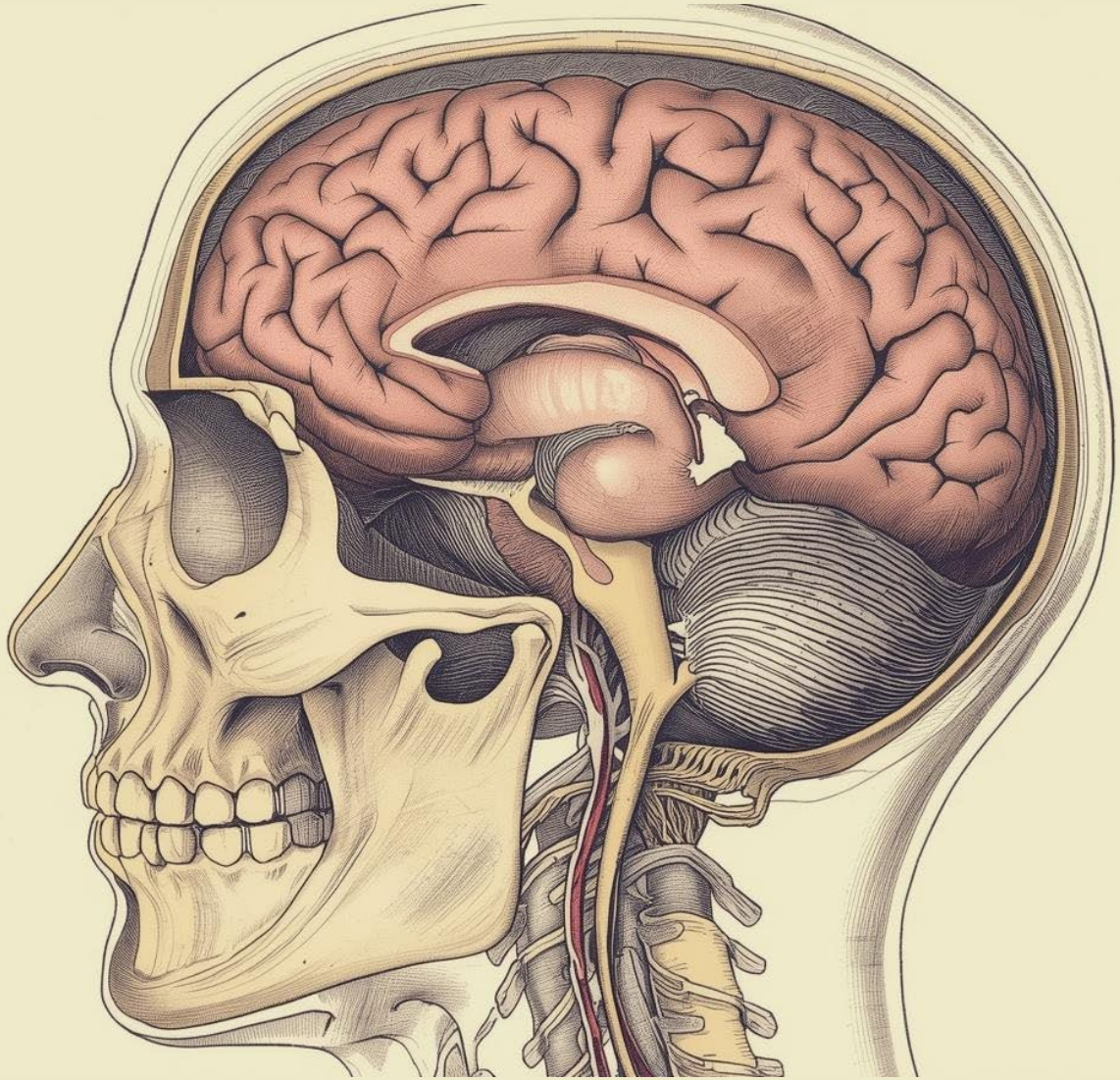

Dopamine
Released in response to an emotionally-charged event, conflict resolution, or pattern recognition. Creates feelings of pleasure.

Cortisol
Released in response to conflict

Oxytocin
Released in response to empathy, connection, compassion, and trust

Reference: www.pamelarutledge.com/story-power-the-psychology-of-story/

Coffee shops opened at 7 AM. The espresso machine was Italian-made. Customer complaints increased 45% in March. A new location opened across the street in February. The barista training program lasted 3 weeks. Average wait time was 12 minutes. Revenue dropped 23% compared to last year. 73% of customers ordered between 7-9 AM. Wait times decreased to 6 minutes by May. The shop had 4 employees. Customer satisfaction scores improved from 3.2 to 4.1. The espresso machine broke down twice per week. Revenue recovered to previous year levels by June.

The little coffee shop on Main Street was struggling. Every morning, loyal customers lined up at 7 AM, but something was wrong. What used to be a quick coffee run had become a frustrating ordeal - broken machines, long waits, and grumpy customers. Then in February, disaster struck: a shiny new competitor opened right across the street. Customers began defecting, and revenue plummeted. The owner faced a choice: give up or fight back. She decided to invest in her people, launching an intensive barista training program in April. Slowly, things turned around. Wait times dropped, smiles returned, and by June, the little shop had not only won back its customers but was thriving more than ever.

The "Story Mountain" Model

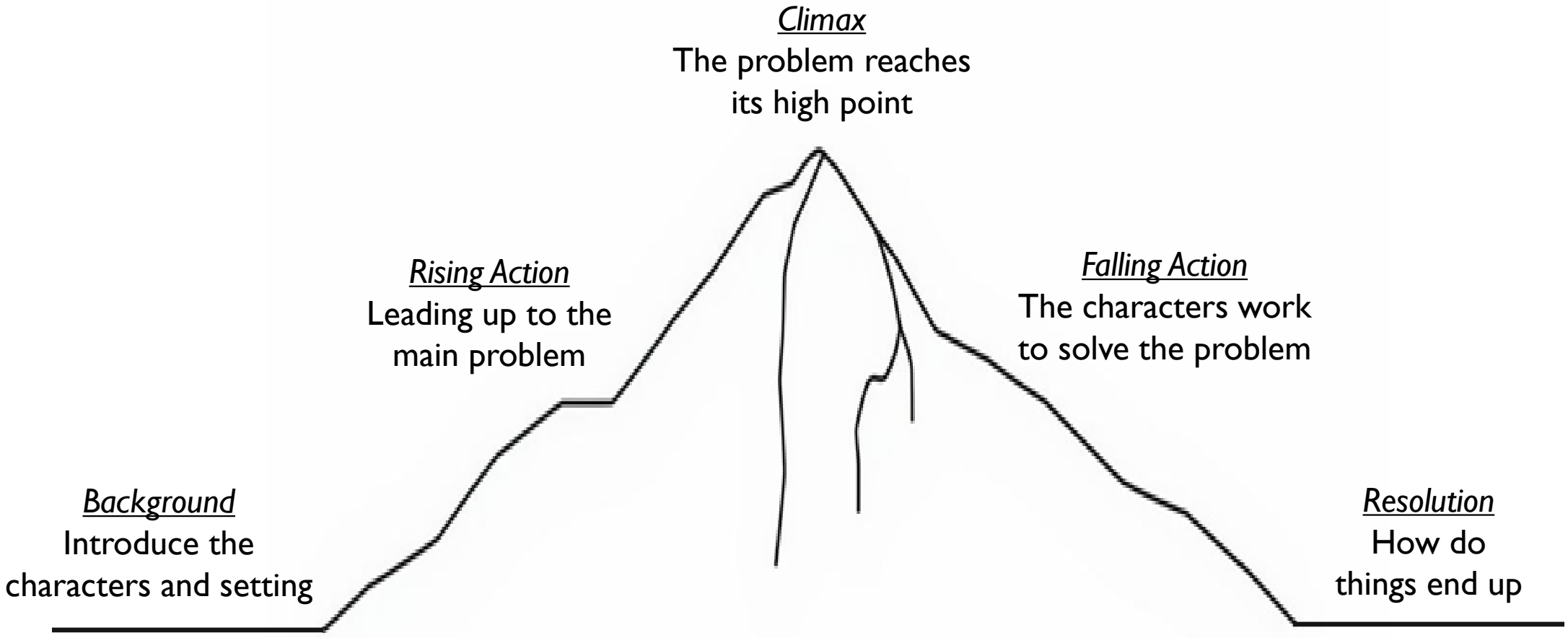

Reference: https://www.studiobinder.com/blog/what-is-a-story-mountain/

The "Story Mountain" Model

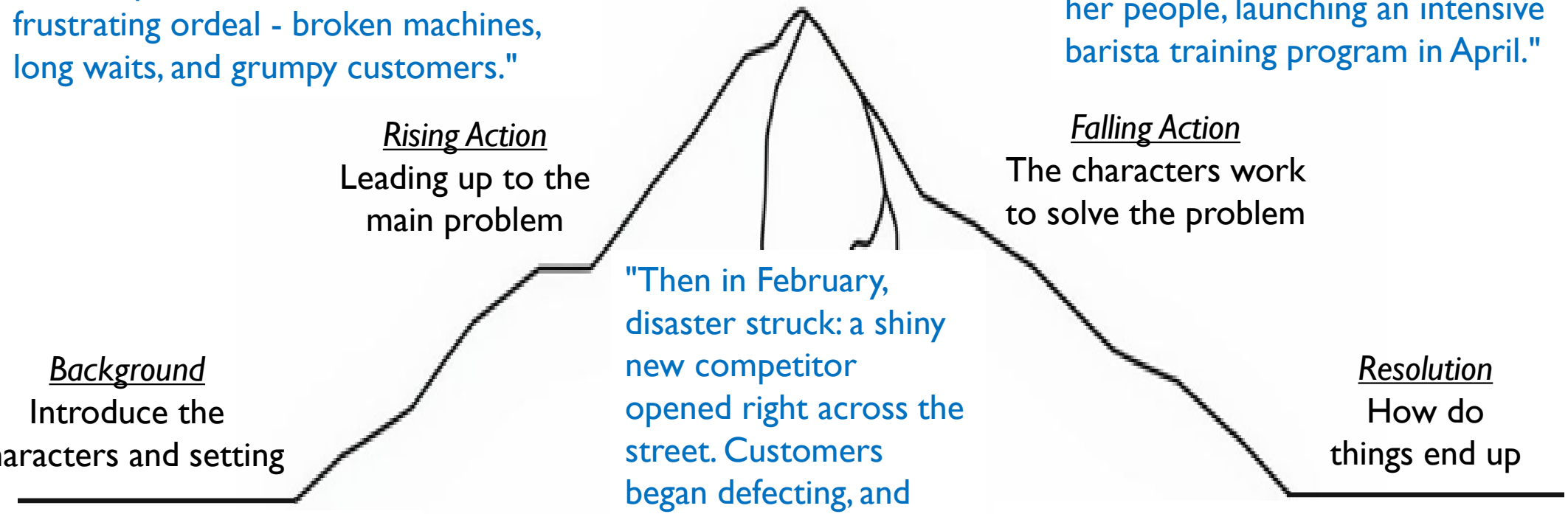

Climax
The problem reaches its high point

"...but something was wrong. What used to be a quick coffee run had become a frustrating ordeal - broken machines, long waits, and grumpy customers."

"The owner faced a choice: give up or fight back. She decided to invest in her people, launching an intensive barista training program in April."

Rising Action
Leading up to the main problem

Falling Action
The characters work to solve the problem

"Then in February, disaster struck: a shiny new competitor opened right across the street. Customers began defecting, and revenue plummeted."

Background
Introduce the characters and setting

Resolution
How do things end up

"The little coffee shop on Main Street was struggling. Every morning, loyal customers lined up at 7 AM..."

"Slowly, things turned around. Wait times dropped, smiles returned, and by June, the little shop had not only won back its customers but was thriving more than ever."

The "Story Mountain" Model

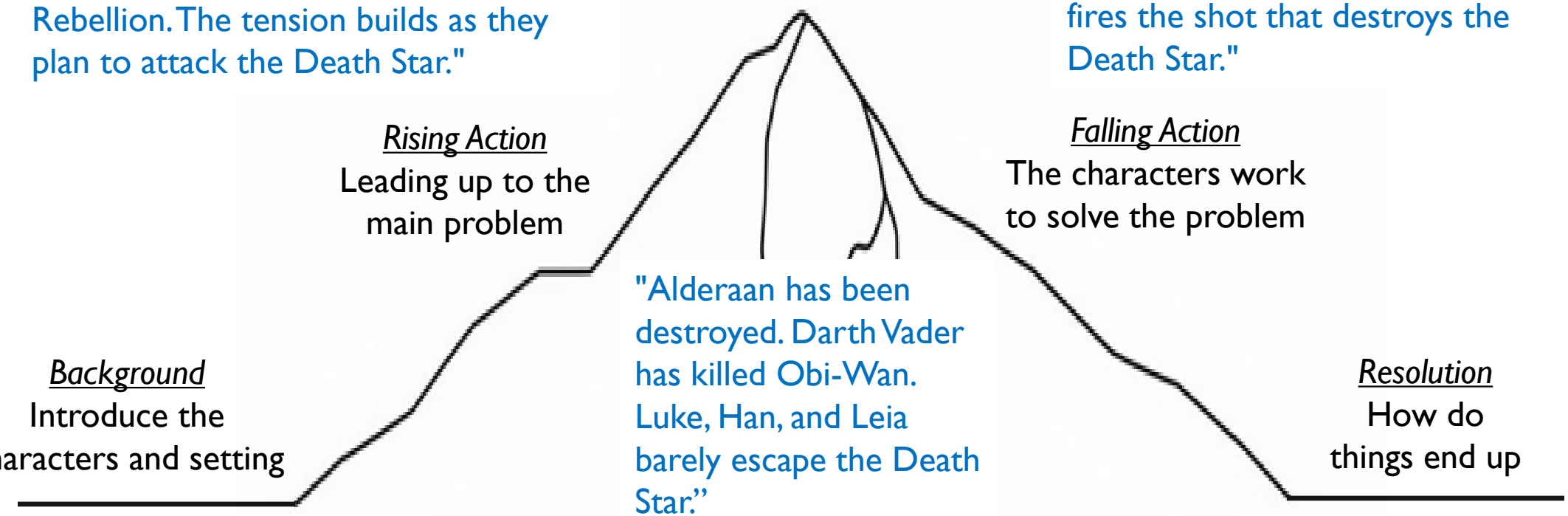

Background
Introduce the characters and setting

"Luke is a farm boy dreaming of adventure. The Empire is oppressing the galaxy, and Princess Leia needs help."

Rising Action
Leading up to the main problem

"Luke discovers his father was a Jedi, meets Obi-Wan, rescues Leia, learns about the Force, and joins the Rebellion. The tension builds as they plan to attack the Death Star."

Climax
The problem reaches its high point

"Alderaan has been destroyed. Darth Vader has killed Obi-Wan. Luke, Han, and Leia barely escape the Death Star."

Falling Action
The characters work to solve the problem

"The rebels attack the Death Star. Luke turns off his targeting computer, trusts the Force, and fires the shot that destroys the Death Star."

Resolution
How do things end up

"The Rebellion celebrates victory, Luke and Han are honored as heroes, hope is restored to the galaxy."

The robot's battery lasted 4 hours. We used aluminum legs. The terrain was rocky with 30-degree slopes. Walking speed was 0.5 meters per second. Previous designs used steel legs. Weight was reduced by 2.3 kg. We tested it outdoors for 3 weeks. The robot had six legs. Power consumption dropped by 40%. We needed it for cave exploration. Temperature range was -10°C to 45°C. Metal alloy cost $120 per leg. We tried nine different leg designs. The robot successfully climbed over 25-cm obstacles. Sensors detected obstacles at 2 meters.

We built a six-legged robot to explore unmapped cave systems. It worked beautifully in our lab tests. But in real caves, we hit a major problem - the battery died after just 90 minutes, right when the robot reached the most interesting unexplored passages. We suspected the heavy steel legs were the culprit, so we tested nine different lightweight materials. When we switched to aluminum alloy, battery life jumped to 4 hours! Our first long mission discovered a chamber we'd never been able to reach before. That 2.3-kg weight reduction transformed everything.

The "Story Mountain" Model

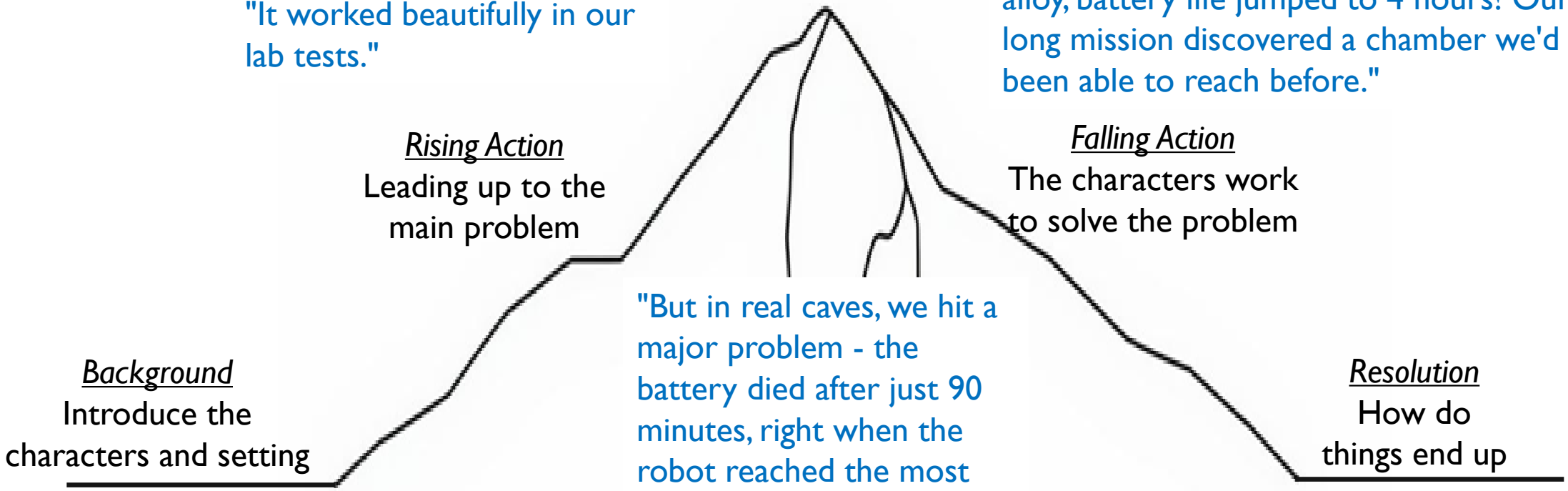

Climax
The problem reaches its high point

"We suspected the heavy steel legs were the culprit, so we tested nine different lightweight materials. When we switched to aluminum alloy, battery life jumped to 4 hours! Our first long mission discovered a chamber we'd never been able to reach before."

"It worked beautifully in our lab tests."

Rising Action
Leading up to the main problem

Falling Action
The characters work to solve the problem

"But in real caves, we hit a major problem - the battery died after just 90 minutes, right when the robot reached the most interesting unexplored passages."

Background
Introduce the characters and setting

Resolution
How do things end up

"We built a six-legged robot to explore unmapped cave systems."

"That 2.3-kg weight reduction transformed everything."

CELL BIOLOGY

ESCRT-mediated membrane repair protects tumor-derived cells against T cell attack

Alex T. Ritter[1*], Gleb Shtengel[2], C. Shan Xu[2], Aubrey Weigel[2], David P. Hoffman[2†], Melanie Freeman[2†], Nirmala Iyer[2], Nensi Alivodej[2‡], David Ackerman[2], Ilia Voskoboinik[3], Joseph Trapani[3], Harald F. Hess[2], Ira Mellman[1*]

CELL BIOLOGY

ESCRT-mediated membrane repair protects tumor-derived cells against T cell attack

Alex T. Ritter[2†], Gleb Shtengel[2], C. Shan Xu[2], Aubrey Weigel[2], David P. Hoffman[2†], Melanie Freeman[2†], Nirmala Iyer[2], Nemsi Alivodej[2‡], David Ackerman[2], Ilia Voskoboinik[3], Joseph Trapani[3], Harald F. Hess[2], Ira Mellman[1*]

Cytotoxic T lymphocytes (CTLs) and natural killer cells kill virus-infected and tumor cells through the polarized release of perforin and granzymes. Perforin is a pore-forming toxin that creates a lesion in the plasma membrane of the target cell through which granzymes enter the cytosol and initiate apoptosis. Endosomal sorting complexes required for transport (ESCRT) proteins are involved in the repair of small membrane wounds. We found that ESCRT proteins were precisely recruited in target cells to sites of CTL engagement immediately after perforin release. Inhibition of ESCRT machinery in cancer-derived cells enhanced their susceptibility to CTL-mediated killing. Thus, repair of perforin pores by ESCRT machinery limits granzyme entry into the cytosol, potentially enabling target cells to resist cytolytic attack.

Cytotoxic T lymphocytes, including cytotoxic T lymphocytes (CTLs) and natural killer (NK) cells, are responsible for identifying and destroying virus-infected or tumorigenic cells. To kill their targets, CTLs and NK cells secrete a pore-forming toxin called perforin through which apoptosis-inducing serine proteases (granzymes) are delivered directly into the cytosol. Successful killing of target cells often requires multiple hits from single or multiple T cells (*1*). This has led to the idea that cytotoxicity is additive, often requiring multiple rounds of sublethal lytic granule secretion events before a sufficient threshold of cytosolic granzyme activity is reached to initiate apoptosis in the target (*2*).

Loss of plasma membrane integrity induced by cytolytic proteins or mechanical damage leads to a membrane repair response. Damage results in an influx of extracellular Ca^{2+}, which has been proposed to lead to the removal of the membrane lesion by endocytosis, resealing of the lesions by lysosomal secretion, or budding into extracellular vesicles (*3*). Perforin pore formation was initially reported to enhance endocytosis of perforin (*4*), but subsequent work has challenged this claim (*5*). Endosomal sorting complexes required for transport (ESCRT) proteins can repair small wounds and pores in the plasma membrane caused by bacterial pore-forming toxins, mechanical wounding, and laser ablation (*6*, *7*). ESCRT proteins are transiently recruited to sites of membrane damage in a Ca^{2+}-dependent fashion, where they assemble budding structures that shed to eliminate the wound and restore plasma membrane integrity. ESCRT-dependent membrane repair has been implicated in the resealing of endogenous pore-mediated plasma membrane damage during necroptosis (*8*) and pyroptosis (*9*).

Localization of target-derived ESCRT proteins to the cytolytic synapse

To investigate whether ESCRT-mediated membrane repair might be involved in the removal of perforin pores during T cell killing, we first determined whether ESCRT proteins in cancer-derived cells were recruited to sites of CTL engagement after perforin secretion. We used CTLs from OT-I mice that express a high-affinity T cell receptor (TCR) that recognizes the ovalbumin peptide SIINFEKL ($OVA_{257-264}$) bound to the major histocompatibility complex (MHC) allele H-2Kb (*10*). We performed live-cell microscopy of OT-I CTLs engaging SIINFEKL-pulsed target cells that express enhanced green fluorescent protein (EGFP)–tagged versions of Tsg101 or Chmp4b, two ESCRT proteins implicated in membrane repair (*6*). To correlate recruitment of ESCRT proteins with perforin exposure in time, we monitored CTL-target interaction in media with a high concentration of propidium iodide (PI), a cell-impermeable fluorogenic dye that can rapidly diffuse through perforin pores to bind and illuminate nucleic acids in the cytosol and nucleus of the target (*5*). EGFP-tagged ESCRT proteins were consistently recruited to the site of CTL-engagement within 30 to 60 s after PI influx (Fig. 1, A and B). EGFP-Tsg101 and EGFP-Chmp4b in target cells accumulated at the cytolytic synapse after PI influx in 25 of 27 (92.6%) and 21 of 33 (63.6%) of conjugates monitored, respectively, compared with a cytosolic EGFP control, which was not recruited (Fig. 1C and movies S1 to S3). Notably, ESCRT-laden material, presumably membrane fragments, frequently detached from the target cell and adhered to the surface of the CTL (Fig. 1, D and E, and movie S2). We observed this phenomenon in ~60% of conjugates imaged in which targets expressed EGFP-Tsg101 or EGFP-Chmp4b (17 of 27 and 20 of 33 conjugates, respectively; Fig. 1D). Shedding of ESCRT-positive membrane from the cell after repair occurs after laser-induced plasma membrane wounding (*6*, *7*). Plasma membrane fragments shed from the target cell into the synaptic cleft likely contain ligands for CTL-resident receptors. Target cell death would separate the CTL and target, revealing target-derived material on the CTL surface.

3D cryo-SIM and FIB-SEM imaging of CTLs caught in the act of killing target cells

Although live-cell imaging indicated that ESCRT complexes were rapidly recruited at sites of T cell–target cell contact, light microscopy alone is of insufficient resolution to establish that this event occurred at the immunological synapse (IS). We thus sought to capture a comprehensive view of the IS in the moments immediately after secretion of lytic granules. We used cryo–fluorescence imaging followed by correlative focused ion beam–scanning electron microscopy (FIB-SEM), which can achieve isotropic three-dimensional (3D) imaging of whole cells at 8-nm resolution or better (*11*–*13*). To capture the immediate response of target cells after perforin exposure, we developed a strategy whereby cryo-fixed CTL-target conjugates were selected shortly after perforation, indicated by the presence of a PI gradient in the target (fig. S1A). In live-cell imaging experiments, PI fluorescence across the nucleus of SIINFEKL-pulsed 1D8 target cells began as a gradient and became homogeneous 158 ± 64 s, on average, after initial PI influx (N = 31 conjugates; fig. S1, B and C, and movie S4). Thus, fixed CTL-target conjugates that exhibited a gradient of PI across the nucleus would have been captured within ~3 min of perforin exposure.

Covenships of CTL-target conjugates underwent high-pressure freezing and were subsequently imaged with wide-field cryogenic fluorescence microscopy followed by 3D cryo-structured illumination microscopy (3D cryo-SIM) performed in a customized optical cryostat (*14*). We selected candidate conjugates for FIB-SEM imaging on the basis of whether a gradient of PI fluorescence was observed across the nucleus of the target emanating from an attached CTL (movie S5). FIB-SEM imaging of the CTL-target conjugate at 8-nm isotropic voxels resulted in a stack of >10,000 individual electron microscopy (EM) images. The image stack was then annotated using a human-assisted machine learning–computer vision platform to segment the plasma membranes of each cell along with cell nuclei and various organelles (https://ariadne.ai/).

We captured four isotropic 3D 8-nm-resolution EM datasets of CTLs killing cancer cells moments after the secretion of lytic granule contents (Fig. 2A and movie S6). Semiautomated segmentation of the cell membranes, nuclei, lytic granules, Golgi apparatus, mitochondria, and centrosomes of the T cells allow for easier visualization and analysis of the 3D EM data. All FIB-SEM datasets and segmentations can be explored online at https://openorganelle.janelia.org (see links in the supplementary materials). Reconstructed views of the segmented data clearly demonstrate the polarization of the centrosome, Golgi apparatus, and lytic granules to the IS—all of which are hallmarks of CTL killing (Fig. 2A, I to iii, and movie S6, time stamp (TS) 1:33) (*15*, *16*). On the target cell side, we noted cytoplasmic alterations consistent with cell damage including enhanced electron density of mitochondria adjacent to the IS (fig. S2A). Close visual scanning of the postsynaptic target cell membrane in the raw EM data failed to reveal obvious perforin pores, which have diameters (16 to 22 nm) close to the limit of resolution for this technique (*17*).

The segmentation of the two cells illustrates the detailed topography of the plasma membrane of the CTL and target at the IS (fig. S2B). The raw EM and segmentation data reveal a dense accumulation of particles, vesicles, and multilamellar membranous materials, which crowd the synaptic cleft between the CTL and the target (Fig. 2B and movie S6, TS 0:40 to 0:50). The source of this intercellular material (IM) was likely in part the lytic granules because close inspection revealed similar particles and dense vesicles located within an-cyt-unreleased granules (fig. S2C). To determine whether some of the membranous material within the intercellular space might also have been derived from the target cell, we examined the surface topology of the postsynaptic target cell. We noted multiple tubular and bud-like protrusions of the target cell membrane that extended into the synaptic space; thus, at least some of the membrane structures observed were still in continuity with the target cell (Fig. 2C and movie S6, TS 0:58 to 1:11). ESCRT proteins have been shown to generate budding structures in the context of plasma membrane repair (*6*), which led us to next assess where target-derived ESCRT proteins are distributed in the context of postsecretion IS.

To map the localization of target-derived ESCRT proteins onto a high-resolution landscape of the IS, we captured three FIB-SEM datasets that have associated 3D cryo-SIM fluorescence data for mEmerald-Chmp4b localization (fig. 3A, fig. S3, and movie S7). This correlative light and electron microscopy (CLEM) revealed that mEmerald-Chmp4b expressed in the target cell was specifically recruited to the target plasma membrane opposite the secreted IM (Fig. 3, B and C). The topography of the plasma membrane at the site of ESCRT recruitment was markedly convoluted, exhibiting many bud-like projections (movie S7, TS 0:37 to 0:40). mEmerald-Chmp4b fluorescence also overlapped with some vesicular structures in the intercellular synaptic space (Fig. 3C). Together, the live-cell imaging and the 3D cryo-SIM and FIB-SEM CLEM demonstrate the localization of ESCRT proteins at the synapse that was the definitive site of CTL killing and was thus spatially and temporally correlated to perforin secretion. These data implicate the ESCRT complex in the repair of perforin pores.

Function of ESCRT proteins in repair of perforin pores

We next investigated whether ESCRT inhibition could enhance the susceptibility of target cells to CTL-mediated killing. Prolonged inactivation of the ESCRT pathway is itself cytotoxic (*9*). We thus developed strategies to ablate ESCRT function that would allow us a window of time to assess CTL killing (fig. S4). We used two approaches to block ESCRT function: CRISPR knockout of the *Chmp4b* gene or overexpression of VPS4a^{E228Q} (E228Q, $Glu^{228} \rightarrow Gln$), a dominant-negative kinase allele that impairs ESCRT function (fig. S4, A to C) (*10*). We took care to complete our assessment of target killing well in advance of spontaneous target cell death (fig. S4D).

We tested the capacity of OT-I CTLs to kill targets presenting one of four previously characterized peptides that demonstrate a range of potencies at stimulating the OT-I TCR: SIINFEKL (N4), the cognate peptide, and three separate variants (in order of highest to lowest affinity), SITFEKL (T4), SIHQFEHL (Q4H7), and SIIGFEKL (G4) (*18*, *19*). Target cells were pulsed with peptide, washed, transferred to 96-well plates, and allowed to adhere before the addition of OT-I CTLs. Killing was assessed by monitoring the uptake of a fluorogenic caspase 3/7 indicator (Fig. 4, A to D, and fig. S5A). Killing was significantly more efficient in ESCRT-inhibited target cells for both CRISPR depletion of Chmp4b (Fig. 4, A to C) and expression of the dominant-negative VPS4a^{E228Q} (Fig. 4D). The difference in killing between the ESCRT-inhibited and control cells was greater when the lower-potency T4, Q4H7, and G4 peptides were used. Nevertheless, ESCRT inhibition moderately improved killing efficiency even in the case of the high-potency SIINFEKL peptide. ESCRT inhibition had no effect on MHC class I expression on the surface of target cells (fig. S5B). B16-F10 cells expressing VPS4a (WT or E228Q) were exposed to increasing concentrations of Prf. Cell viability was determined by morphological gating (E), FSC, forward scatter; SSC, side scatter; (**G** and **H**) B16-F10 cells expressing VPS4a (WT or E228Q) were exposed to a sublytic dose of Prf in combination with increasing concentrations of recombinant GZMB (rGZMB). Cell death was determined by Annexin V–allophycocyanin (APC) staining (G). Controls include a condition with no perforin and 5000 ng/ml rGZMB and subtlytic perforin with no rGZMB. Graphs in (F) and (H) represent the means of three experiments, and error bars indicate SDs. Statistical significance was determined by multiple unpaired t tests with alpha = 0.05. ns, not significant; *P < 0.05, **P < 0.01; ***P < 0.001.

Downloaded from https://www.science.org on September 26, 2025

[1]Genentech, Inc., South San Francisco, CA 94080, USA. [2]Janelia Research Campus, Howard Hughes Medical Institute, Ashburn, VA 20147, USA. [3]Rosie Lew Cancer Immunology Program, Peter MacCallum Cancer Centre, Melbourne VIC, Australia.
*Corresponding author. Email: ritter.alex@gene.com (A.T.R.); ira@gene.com (I.M.)
†Present address: 10X Genomics, Inc., Pleasanton, CA 94566, USA. ‡Present address: Neurovascular Interface, Goethe University Frankfurt and Max Planck Institute for Brain Research, 60438 Frankfurt am Main, Germany.

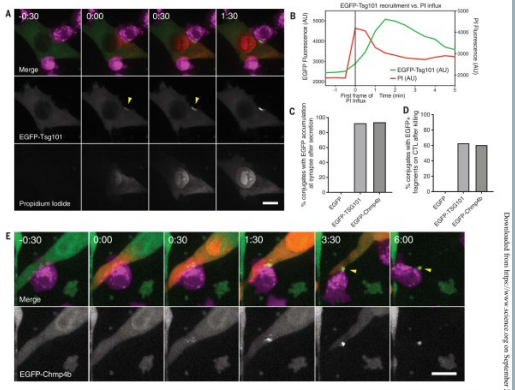

Fig. 1. Fluorescently tagged ESCRT proteins in targets localize to site of CTL killing after perforin secretion. (**A**) Live-cell spinning disk confocal imaging of a fluorescently labeled OT-I CTL (magenta) engaging an MC38 cancer cell expressing EGFP-Tsg101 (green) in media containing 100 μM PI (red). Yellow arrowheads highlight ESCRT recruitment. T 0:00 is the first frame of PI influx into the target cell (time in minutes:seconds). Scale bar, 10 μm. (**B**) Graph of EGFP-Tsg101 and PI fluorescence intensity at the IS within the target over time, from example in (A). AU, arbitrary units. (**C** and **D**) Quantification of CTL-target conjugates exhibiting accumulation of EGFP at the synapse after PI influx (C) or detectable EGFP-labeled material associated with CTL after target interaction (D) (EGFP condition: N = 22 conjugates in seven independent experiments; EGFP-Tsg101 condition: N = 27 conjugates in nine independent experiments; EGFP-Chmp4b condition: N = 33 conjugates in 24 independent experiments). (**E**) Live-cell spinning disk confocal imaging of OT-I CTL (magenta) killing MC38 expressing EGFP-Chmp4b (green), demonstrating the presence of target-derived EGFP-Chmp4b material (yellow arrowheads) associated with CTL membrane after a productive target encounter. T 0:00 is the first frame of PI influx into the target cell. Scale bar, 10 μm.

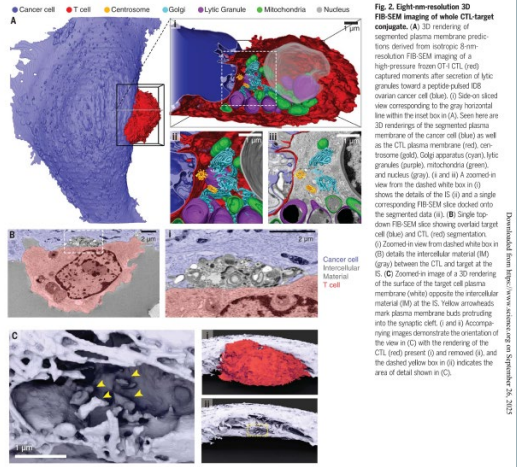

Fig. 2. Eight-nm-resolution 3D FIB-SEM imaging of whole CTL-target conjugate. (**A**) 3D rendering of segmented plasma membrane predictions derived from isotropic 8-nm-resolution FIB-SEM imaging of a high-pressure frozen OT-I CTL (red) captured moments after secretion of lytic granules toward a peptide-pulsed 1D8 ovarian cancer cell (blue). (i) Side-on sliced view corresponding to the gray horizontal line within the inset box in (A). Seen here are 3D renderings of the segmented plasma membrane of the cancer cell (blue) as well as the CTL plasma membrane (red), centrosome (gold), Golgi apparatus (cyan), lytic granules (purple), mitochondria (green), and nucleus (gray). (ii and iii) A zoomed-in view from the dashed white box in (i) shows the details of the IS (ii) and a single corresponding FIB-SEM slice docked onto the segmented data (iii). (**B**) Single top-down FIB-SEM slice showing overlaid target cell (blue) and CTL (red) segmentation. (i) Zoomed-in view from dashed white box in (B) details the intercellular material (IM) (gray) between the CTL and target at the IS. (**C**) Zoomed-in image of a 3D rendering of the surface of the target cell plasma membrane (white) opposite the intercellular material (IM) at the IS. Yellow arrowheads mark plasma membrane buds protruding into the synaptic cleft. (i and ii) Accompanying images demonstrate the orientation of the view in (C) with the rendering of the CTL (red) present (i) and removed (ii), and the dashed yellow box in (ii) indicates the area of detail shown in (C).

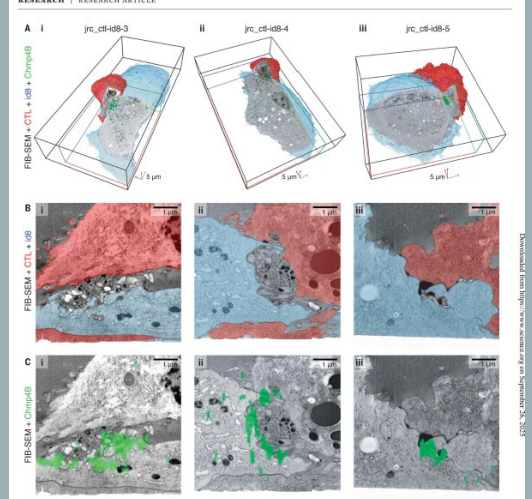

Fig. 3. Correlative 3D cryo-SIM and FIB-SEM reveal localization of target-derived ESCRT within the cytolytic IS. (**A**) Three example datasets showing correlative 3D cryo-SIM and FIB-SEM imaging of OT-I CTLs (red) captured moments after secretion of lytic granules toward peptide-pulsed 1D8 cancer cells (blue) expressing mEmerald-Chmp4b (green fluorescence). (**B** and **C**) Single FIB-SEM slices corresponding to the orange boxes in (A), overlaid with CTL and cancer cell segmentation (B) or correlative cryo-SIM fluorescence of mEmerald-Chmp4b derived from the target cell (C).

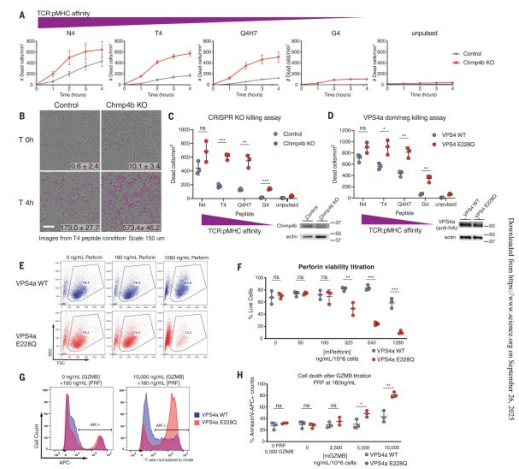

Fig. 4. ESCRT inhibition enhances susceptibility of cancer cells to CTL killing and recombinant lytic proteins. (**A**) Representative time-lapse data of killing of peptide-pulsed Chmp4b knockout (KO) or control B16-F10 cells by OT-I CTLs. Affinity of the pulsed peptide to OT-I TCR decreases from left to right. Error bars indicate SDs. (**B**) Images extracted from T4 medium-affinity peptide condition show software-detected caspase 3/7+ events in control and Chmp4b KO conditions. (**C** and **D**) Data representing the 4-hour time point of assays measuring OT-I T cells killing either Chmp4b KO (C) or VPS4 dominant-negative (D) target cells with matched controls. Error bars indicate SDs of data. Data are representative of at least three independent experimental replicates. pMHC, peptide-MHC; HA, hemagglutinin. (**E** and **F**) Determination of sublytic dose of Prf. B16-F10 cells expressing VPS4a (WT or E228Q) were exposed to increasing concentrations of Prf, and cell viability was determined by morphological gating (E), FSC, forward scatter; SSC, side scatter, (**G** and **H**) B16-F10 cells expressing VPS4a (WT or E228Q) were exposed to a subtlytic dose of Prf in combination with increasing concentrations of recombinant GZMB (rGZMB). Cell death was determined by Annexin V–allophycocyanin (APC) staining (G). Controls include a condition with no perforin and 5000 ng/ml rGZMB and subtlytic perforin with no rGZMB. Graphs in (F) and (H) represent the means of three experiments, and error bars indicate SDs. Statistical significance was determined by multiple unpaired t tests with alpha = 0.05. ns, not significant; *P < 0.05, **P < 0.01; ***P < 0.001.

Thus, ESCRT inhibition could sensitize target cells to perforin- and granzyme-mediated killing, especially at physiologically relevant TCR-peptide MHC affinities.

We next directly tested the effects of ESCRT inhibition when target cells were exposed to both recombinant perforin (Prf) and granzyme B (GZMB), the most potently proapoptotic granzyme in humans and mice (*20*). Prf alone at high concentrations can lyse cells (*4*), so we first determined a sublytic Prf concentration that would temporarily permeabilize the plasma membrane but permit the cells to recover. B16-F10 cells expressing either VPS4a^{WT} (WT, wild-type) or VPS4a^{E228Q} were exposed to a range of Prf concentrations in the presence of PI, and cell viability and PI uptake were assessed using flow cytometry. Cells that expressed dominant-negative VPS4a^{E228Q} were more sensitive to Prf alone than ESCRT-competent cells (Fig. 4, E and F). At 100 ng/ml Prf, there was no significant difference in cell viability for either condition. Cells in the live gate that were PI+ had been permeabilized by Prf but recovered. Although the percentage of PI+ live cells was similar under both sets of conditions, the mean fluorescence intensity of PI was higher in live ESCRT-inhibited cells (fig. S6). A delay in plasma membrane resealing could account for this difference.

We reasoned that delaying perforin pore repair might also enhance GZMB uptake into the target. ESCRT-inhibited cells were more sensitive to combined perforin-GZMB when cell death was measured by Annexin V staining (Fig. 4, G and H). Similar results were observed when these experiments were repeated with a murine lymphoma cancer cell line (fig. S7). The observation that ESCRT-inhibited target cells are more sensitive to both CTL-secreted and Prf-GZMB supports the hypothesis that the ESCRT pathway contributes to membrane repair after Prf exposure.

Escaping cell death is one of the hallmarks of cancer. Our findings suggest that ESCRT-mediated membrane repair of perforin pores may restrict accessibility of the target cytosol to CTL-secreted granzyme, thus promoting survival of cancer-derived cells under cytolytic attack. Although other factors may contribute to setting the threshold for target susceptibility to killing, the role of active repair of perforin pores must now be considered as a clear contributing factor.

REFERENCES AND NOTES

1. S. Halle *et al.*, *Immunity* **44**, 233–245 (2016).
2. B. Wagakin *et al.*, *Nat. Commun.* **12**, 5217 (2021).
3. N. W. Andrews, P. E. Almeida, M. Corrotte, *Trends Cell Biol.* **24**, 734–742 (2014).
4. D. Keefe *et al.*, *Immunity* **23**, 249–262 (2005).
5. J. A. Lopez *et al.*, *Blood* **121**, 2659–2668 (2013).
6. A. J. Jimenez *et al.*, *Science* **343**, 1247138 (2014).
7. L. L. Scheffer *et al.*, *Nat. Commun.* **5**, 5646 (2014).
8. Y.-N. Gong *et al.*, *Cell* **169**, 286–300.e16 (2017).
9. S. Rühl *et al.*, *Science* **362**, 956–960 (2018).
10. K. A. Hogquist *et al.*, *Cell* **76**, 17–27 (1994).
11. G. Knott, H. Marchman, D. Wall, B. Lich, *J. Neurosci.* **28**, 2959–2964 (2008).
12. C. S. Xu *et al.*, *eLife* **6**, e25916 (2017).
13. C. S. Xu *et al.*, *Nature* **599**, 147–151 (2021).
14. D. P. Hoffman *et al.*, *Science* **367**, eaaz5357 (2020).
15. A. T. Ritter *et al.*, *Immunity* **42**, 864–876 (2015).
16. J. C. Stinchcombe, E. Majorovits, G. Bossi, S. Fuller, G. M. Griffiths, *Nature* **443**, 462–465 (2006).
17. I. Voskoboinik, J. C. Whisstock, J. A. Trapani, *Nat. Rev. Immunol.* **15**, 388–400 (2015).
18. M. A. Daniels *et al.*, *Nature* **444**, 724–729 (2006).
19. A. C. Richard *et al.*, *Nat. Immunol.* **19**, 849–858 (2018).
20. D. Kaiserman *et al.*, *J. Cell Biol.* **175**, 619–630 (2006).

ACKNOWLEDGMENTS

We thank members of the Mellman laboratory for advice, discussion, and reagents; B. Haley for assistance with plasmid construct design; the Genentech FACS Core Facility for technical assistance; S. Van Engelenburg of Denver University for invaluable discussions and guidance; A. Weimer, S. Spier, and the Ariande AI AG (https://ariadne.ai/) for assistance with FIB-SEM segmentation. CLEM coregistration, data presentation, and rendering; D. Bennett of the Janelia Research Campus for assisting with data upload to https://openorganelle.janelia.org; and the Genentech Postdoctoral Program for support.
Funding: A.T.R. and I.M. are funded by Genentech/Roche. C.S.X., S.G., A.W., D.A., N.I., and H.F.H. are funded by The Howard Hughes Medical Institute (HHMI). **Author contributions:** A.T.R. designed and performed experiments and analyzed the data; A.T.R. and I.M. wrote the manuscript with input from all coauthors. G.S. and M.F. performed high-pressure freezing. G.S., D.P.H., and N.A. collected cryo–fluorescence images. G.S. and N.I. performed freeze-substitution and resin embedding. G.S. prepared samples for FIB-SEM. G.S. and C.S.X. conducted FIB-SEM imaging. C.S.X. processed FIB-SEM data. D.A. and A.W. developed FIB-SEM data analysis. D.A. performed FIB-SEM data analysis. A.W. prepared figs. 1 and 3. I.V. and J.T. provided valuable reagents and consulted on experiments. M.F.H. and I.M. supervised the work and provided support. **Competing interests:** A.T.R. and I.M. declare that they are Genentech/Roche employees. C.S.X. and H.F.H. are the inventors of a US patent assigned to HHMI for the enhanced FIB-SEM systems used in this work ("Enhanced FIB-SEM systems for large-volume 3D imaging." US Patent 10,600,615). The authors declare no other competing interests. **Data and materials availability:** All data are available in the main text or the supplementary materials. Full FIB-SEM datasets and segmentations are freely available to be explored on https://openorganelle.janelia.org, with direct links and data accession numbers provided in the supplementary materials. Cell lines and plasmids are available from I.M. upon request.

SUPPLEMENTARY MATERIALS

science.org/doi/10.1126/science.abl5855
Materials and Methods
Figs. S1 to S7
References (21–25)
MDAR Reproducibility Checklist
Movies S1 to S7

View/request a protocol for this paper from *Bio-protocol*.

9 July 2021; resubmitted 22 December 2021
Accepted 4 March 2022
10.1126/science.abl5855

RESEARCH

CELL BIOLOGY

ESCRT-mediated membrane repair protects tumor-derived cells against T cell attack

Alex T. Ritter[1]*, Gleb Shtengel[2], C. Shan Xu[2], Aubrey Weigel[2], David P. Hoffman[2]†, Melanie Freeman[2]†, Nirmala Iyer[2], Nensi Alivodej[2]‡, David Ackerman[2], Ilia Voskoboinik[3], Joseph Trapani[3], Harald F. Hess[2], Ira Mellman[1]*

Background (Setting the scene)

Our immune system has special "killer" cells whose job is to find and destroy dangerous cells — like cancer cells. These killer cells attack by shooting tiny protein bullets called **perforin**, which punch holes in the target cell's outer membrane. Through those holes, they send in enzymes called **granzymes**, which trigger the cell to self-destruct.

Rising Action (Why this matters now)

But scientists noticed something puzzling: immune cells often need to attack the same target many times before it dies. Sometimes the cancer cell survives repeated assaults. Could the cancer cells be fighting back in some way?

Climax (The big problem revealed)

The researchers discovered that tumor cells can **repair the very holes perforin makes**! They use a built-in emergency repair crew of proteins called **ESCRT proteins**, which rush to the wound site and patch it up within seconds. That means the cancer cell plugs the holes before enough of the deadly granzymes can slip inside.

Falling Action (The discovery)

Using powerful microscopes, the scientists actually watched this process in action. They saw the repair proteins gathering at the immune attack sites, cutting off and shedding damaged membrane, and restoring the cell's surface. But when the researchers blocked this ESCRT repair system, cancer cells became much easier for immune cells to kill.

Resolution (Why it matters)

This finding changes how we think about the fight between the immune system and cancer. It shows that cancer cells don't just passively endure attack — they actively defend themselves by repairing the damage. And it suggests a new way forward: if scientists can design drugs that slow or block this repair system, they may make cancer cells far more vulnerable to our body's natural defenses. In other words, stopping the patchwork crew could help unleash the full power of the immune system.

Your turn to tell a story…

With your group:

- Look over your article (QR code)
- Read the facts on the fact sheets
- Decide which facts are most important to your story and the order in which they should be placed

YOU CAN USE NO MORE THAN 5 FACTS PER SECTION

(Only include the information that helps tell your story!)

- Use scissors to cut out the facts you want to use
- Tape your facts together in the order you plan to tell the story
- **Add connecting words and** phrases **like *then, but, therefore, however, as a result, etc***
- Be prepared to read your story

#1

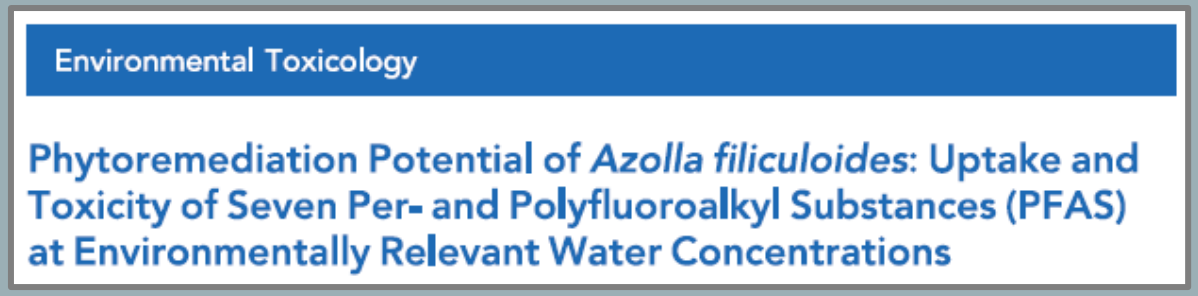

#2

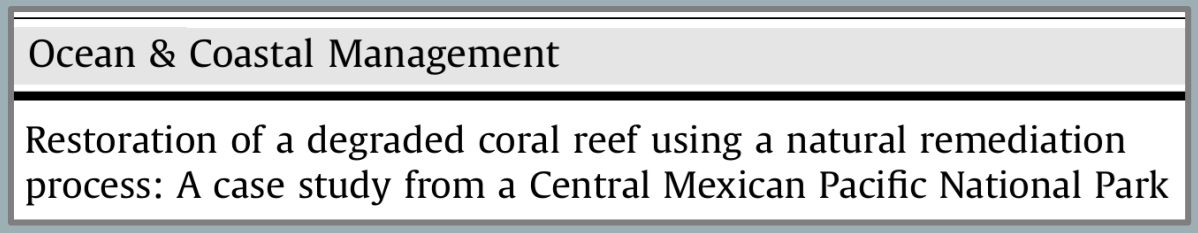

#3

Access articles and fact sheets:

Provide Your Feedback on:
The Art of Scientific Storytelling: Crafting Compelling STEM Presentations

Survey Link:
https://airtable.com/appMqgBJxZT21jAQH/pagtWLpTyNMqVPVc8/form